Qi *et al. BioData Mining* (2026) 19:40
https://doi.org/10.1186/s13040-026-00542-4

BioData Mining

RESEARCH Open Access

Metabolic reprogramming of tumor-associated macrophage clusters in ovarian cancer: a single-cell transcriptomic analysis and prognostic model

Lin Qi[1†], Li Li[2†], Yinuo Liu[3], Wenshu Li[1], Yaru Ma[4*†] and Manyin Zhao[1*†]

[†]Lin Qi, Li Li and Yinuo Liu contributed equally to this work and should be considered as co-first authors.

[†]Yaru Ma and Manyin Zhao contributed equally to this work and should be considered co-corresponding authors.

*Correspondence:
Yaru Ma
qdmayaru@163.com
Manyin Zhao
zmy5168@sina.com
[1]Department of Gynecology and Obstetrics, Yantai Yuhuangding Hospital Affiliated to Qingdao University, No. 20, Yuhuangding East Road, Zhifu District, Yantai, Shandong 264000, China
[2]Department of Gynecology, Hunan Cancer Hospital, Changsha, Hunan 410013, China
[3]Qingdao Medical College of Qingdao University, Qingdao, Shandong 266000, China
[4]Department of Gynecology, The Women and Children's Hospital of Qingdao University, 217 Liaoyang West Road, Qingdao, Shandong 266000, China

Abstract

Purpose The complex tumor microenvironment (TME) in ovarian cancer (OC), particularly the role of macrophage clusters, plays a pivotal role in driving cancer progression and determining patient prognosis. Metabolic reprogramming is a hallmark of tumorigenesis and is crucial in reshaping the TME and driving tumor progression.

Methods Through a comprehensive single-cell RNA sequencing analysis of macrophage clusters in OC, this study integrated data from four independent datasets and identified hypermetabolic subpopulations within nine distinct mononuclear phagocyte clusters.

Results The identified clusters were notably enriched in pathways related to the TCA cycle, glycolysis, and HIF-1 signaling, which are closely linked to tumor invasiveness and immune modulation. Transcriptional regulation analysis revealed key drivers of these metabolic changes, including ZNF574, BRCA1, and ATF5, which might be potential therapeutic targets. Cell-cell communication analysis demonstrated that hypermetabolic macrophage clusters engaged in extensive signaling with tumor epithelial cells, thereby influencing the immune TME and potentially contributing to immune evasion. A metabolism-related prognostic model was also established based on differentially expressed genes within hypermetabolic macrophages, which exhibited robust predictive power for overall survival in OC patients.

Conclusions Our findings reveal strong associations between metabolic reprogramming in tumor-associated macrophages and OC progression, suggesting their potential importance in shaping the TME. This study provides novel insights into possible therapeutic strategies and prognostic tools for OC, which warrant further functional validation.

Clinical trial number Not applicable.

Keywords Ovarian cancer, Metabolic reprogramming, Tumor-associated macrophages, Single-cell RNA sequencing, Tumor microenvironment, Prognostic model

Introduction

Ovarian cancer (OC) is a lethal gynecological malignancy worldwide, with high mortality rates primarily due to late-stage diagnosis and resistance to conventional therapies [1]. This aggressive malignancy typically presents at advanced stages, with approximately 75% of cases diagnosed after metastasis (stages III and IV) [2]. Patients with advanced OC exhibit a dismal five-year survival rate, hovering around 30% [3]. A better understanding of the tumor microenvironment (TME) is essential for developing novel therapeutic strategies for OC.

Within the complex and multifaceted TME of OC, immune cells are particularly prominent among multiple critical components, which may either promote or block tumor progression [4]. Notably, tumor-associated macrophages (TAMs) represent an abundant population and are known to stimulate tumor progression and chemoresistance [5]. Macrophages within the TME exhibit notable plasticity and can polarize into distinct phenotypes according to the local signals they encounter [6]. These phenotypes are typically classified into two main categories: the classically activated M1 macrophages, which boast anti-tumor properties, and the alternatively activated M2 macrophages, which promote tumor growth, angiogenesis, and immune suppression [7]. Hence, it is essential to elucidate the roles of different macrophage subtypes in OC.

Single-cell RNA sequencing (scRNA-seq) is an established powerful tool that unveils cellular heterogeneity within tumors at an unprecedented resolution [8]. This technology can identify rare cell populations, map cellular developmental trajectories, and analyze intercellular communication [9]. Recent advances in scRNA-seq have provided novel ideas for cellular compositions and diverse functions of the OC TME. In particular, scRNA-seq investigations have unveiled the heterogeneity of TAMs within the OC TME and revealed macrophage clusters with distinct metabolic and immunological properties [10]. These findings suggest that it is necessary to gain insight into the molecular mechanisms of macrophage heterogeneity and its role in OC progression. Our analysis reveals metabolic reprogramming in mononuclear phagocyte clusters (MPCs) in OC at the single-cell level, showing significant enrichment in TCA cycling, fatty acid metabolism, and amino acid metabolism. These metabolic pathways facilitate rapid tumor growth and increase resistance to platinum-based drugs.

Metabolic reprogramming, similar to TAMs, is a hallmark of cancers. Macrophages within the TME frequently experience metabolic shifts that support tumor progression. For example, TAMs can switch from oxidative phosphorylation to glycolysis in response to hypoxia within the tumor, thus promoting tumor growth and immune evasion [11]. Hypermetabolic TAMs, in particular, support tumor cell proliferation and invasion by secreting pro-inflammatory cytokines and growth factors. Analyzing the metabolic reprogramming of TAMs in OC could uncover new therapeutic strategies, as targeting key metabolic pathways may disrupt the supportive role of macrophages in tumor progression. Metabolic reprogramming in OC promotes the survival and proliferation of cancer cells, improves their adaptation to unfavorable environments, and stimulates immune escape and tumor progression. Targeting metabolic reprogramming has been used to enhance the anti-tumor efficacy of lysosomal viral therapy for OC by modulating energy metabolism within cancer or immune cells.

OC treatment is mainly limited by chemoresistance. TAMs promote chemoresistance through various mechanisms, for example, secreting cytokines interleukin (IL)-6

and tumor necrosis factor-α (TNF-α), which activate survival pathways in tumor cells [12]. TAMs can also promote chemoresistance by enhancing drug efflux transporters and anti-apoptotic proteins in cancer cells [13]. Hence, targeting TAMs can curb tumor growth and overcome chemoresistance. Emerging therapies that aim at reprogramming TAMs from a pro-tumorigenic (M2-like) to an anti-tumorigenic (M1-like) phenotype are investigated to enhance the efficacy of existing treatments. Several studies have stated that primary tumor growth and metastasis of breast cancer and OC can be effectively inhibited using Toll-like receptor (TLR) agonists in combination with interferon gamma (IFNγ). This strategy enhances the immune response to tumors by promoting the polarization of M1 macrophages [14]. In terms of immunotherapy for OC, a prospective clinical trial has revealed the differences in the TME between homologous recombination repair-deficient and homologous recombination repair-intact OC based on multi-omics data from and has provided new targets for immunotherapy and combination regimens for homologous recombination repair-deficient OC. This suggests that the effect of immunotherapy can be enhanced by remodeling the TME [15].

In summary, the TME of OC is highly dynamic and complex and is critical in tumor progression and chemoresistance. TAMs are crucial components of the TME, exhibiting significant plasticity and functional diversity. The scRNA-seq technology has offered new insights into the heterogeneity of TAMs within OC, revealing distinct macrophage clusters with varying metabolic and immunological properties. Understanding the molecular mechanisms of TAM heterogeneity and their interplays with other cells in the TME is essential for developing novel strategies for reprogramming the immune microenvironment and improving OC patient outcomes.

Materials and methods

Public data sources

The public scRNA-seq datasets (GSE154600, GSE158937, GSE184880, GSE165897) and bulk RNA-seq (GSE26712) were downloaded from the Gene Expression Omnibus database (https://www.ncbi.nlm.nih.gov/geo). The expression dataset from bulk RNA-seq and the dataset of TCGA OC phenotypes were downloaded from UCSC Xena [16] (http://xena.ucsc.edu/).

Quality control and data integration

Cells were filtered for detected genes (300–7000), mitochondrial gene percent (0–50%), hemoglobin gene percent (0–10%), unique molecular identifier (1000–30000), and ribosomal gene percent (min: 1–50%). Genes that were expressed in fewer than 3 cells were removed. Doublet cells (doublet) were removed in batches via the scDblFinder.

Reciprocal principal component analysis was performed to correct batch effects in data [17]. The FindVariableFeatures function in the Seurat package was utilized to pinpoint the top 2000 highly variable genes [18], with default parameters. Principal component analysis was performed with these variable genes after Z-score normalization. Dimensionality reduction was performed using uniform manifold approximation and projection (UMAP) with the top 30 significant principal components. Additionally, clusters were examined using the FindClusters function (resolution = 0.3). Marker genes with a fold change > 2 were identified for each cluster using the Seurat FindMarkers function. Cell types were annotated with marker genes using CellMarker 2.0 [19] and

PanglaoDB [20]. Subclustering analysis was performed on the MPC population after integration across samples. Clustering was conducted at multiple resolutions (0.01–1.2), and resolution 0.3 was selected based on cluster separation and marker gene expression. Marker genes were identified using FindAllMarkers, with logfc.threshold ≥ 0.5 and $p <$ 0.05 (Bonferroni-corrected).

Gene set variation functional analysis (GSVA)

GSVA analyses were conducted with clusterProfiler [21] and AddModuleScore functions in the Seurat package. Hallmark, Kyoto Encyclopedia of Genes and Genomes (KEGG) [22], and Reactome pathway databases obtained from R package msigdbr (http://www.gsea-msigdb.org/gsea/msigdb/) were applied for GSVA analyses.

Pseudotime analysis

Single-cell pseudotime trajectory of Slingshot [23] was constructed using R package SCP. The RunSlingshot function was adopted to derive trajectories; the FeatureDimPlot function was utilized to plot the trajectories downscaled; subsequently, the genes over pseudotime were identified by the RunDynamicFeatures function and visualized by DynamicHeatmap.

Cell-cell communication analysis

R package CellChat was employed for cell-cell communication analysis [24], with a minimum cell number of 10. 500 cells from each cluster were randomly selected using the subset function. Secreted Signaling, ECM-Receptor, and Cell-Cell Contact in the Cellchat database were used.

TCGA and TME analysis

The overall survival (OS) was determined with the survival package (R package 3.4) using the log-rank test. The BayesPrism algorithm was utilized to infer the scRNA-seq datasets. BayesPrism is a sophisticated Bayesian inference tool designed to extract detailed information from scRNA-seq data and map this information onto bulk RNA-seq data. This process can infer both the cellular composition and gene expression profiles within the TME. In the TME, immune cells and stromal cells are two primary types of normal cells. An estimate algorithm can predict their scores using the expression data and calculate tumor purity in each tumor sample [25]. The ESTIMATE score, immune score, stromal score, and tumor purity of different clusters were computed via the estimate R package [26].

Establishment and validation of the prognostic risk model

LASSO analysis was employed to identify prognostic biomarkers in the TCGA-OC cohort. Then, univariate Cox analysis was utilized to select the final variables. Ten MPC-related genes were verified as significant hub genes with $P < 0.05$. The prognostic risk model was constructed and shown in forest plots. The risk score was computed: risk score = β1* Gene1 Expression Level + β2* Gene2 Expression Level + … + βx* GeneX Expression Level (β represents the regression coefficient). The Kaplan–Meier curves and time-dependent receiver operating characteristic (ROC) curves were drawn to check the clinical accuracy.

Statistical analyses

R software 4.1.3 was applied for statistical analyses, and p-values and FDR (false discovery rate) q-values < 0.05 implied statistical differences.

Results

Characterization of the single-cell transcriptomic landscape of macrophage clusters in OC

scRNA-seq data were integrated from four datasets (GSE154600, GSE158937, GSE184880, GSE165897) related to OC. After removing batch effects and implementing rigorous quality control, we retained 136,193 high-quality cells for further analysis. Dimensionality reduction and clustering identified 17 clusters (Supplementary Fig. 1A-D). Cell annotation based on marker genes revealed 14 distinct cell types (Fig. 1A), including mast cells, dendritic cells, MPC cells, plasma cells, B cells, CD8 T cells, CD4 T cells, gamma delta T cells, stromal cells, vascular smooth muscle cells, fibroblasts, endothelial cells, Sertoli cells, and epithelial cells. Marker genes for these cell types are shown in Fig. 1B. The optimal clustering resolution of 0.3 was selected based on a systematic evaluation of the trade-off between cluster separation (silhouette) and granularity (cluster count) (Supplementary Fig. 2). MPCs were further extracted for in-depth analysis, and the clustering of 19,544 MPCs identified 9 distinct clusters (Fig. 1C-D). Analysis of differentially expressed genes (DEGs) in these clusters showed that MPC1 and MPC2 primarily exhibited characteristics of ovarian resident MPCs; MPC3, MPC5, and MPC7 were characteristic of TAMs; MPC4 exhibited monocyte features; and MPC6, MPC8, and MPC9 exhibited dendritic cell characteristics (Fig. 1E). The screening criteria for differential analysis were $|avg\_log2FC| > 0.5$ and FDR < 0.05. In summary, we for the first time depict the single-cell landscape of macrophage clusters in OC.

Functional differences among MPCs

Tumor progression is characterized by malignant transformation in key cancer hallmarks, including cellular metabolism, signal transduction, cell proliferation, and apoptosis [27]. Gene ontology (GO), KEGG, and WikiPathway analyses of DEGs across 9 MPCs (Fig. 2A) revealed significant functional differences. Clusters MPC1, MPC4, MPC6, MPC8, and MPC9 were predominantly associated with immune responses, showing enrichment in the IL-17, hypoxia-inducible factor-1 (HIF-1), and NF-kappa B signaling pathways. MPC3 was notably enriched in pathways related to cellular metabolism, including the TNF and IL-17 pathways. MPC5 was primarily associated with cell proliferation pathways, like the cell cycle and DNA replication. MPC7, enriched in the HIF-1 pathway, glycolysis, and gluconeogenesis, was potentially linked to apoptosis and metabolic reprogramming. Pathways were screened based on FDR < 0.05. The analysis of marker genes for each subpopulation (Fig. 2B-C) and their regulatory gene networks (Supplementary Fig. 3) indicated that MPCs were different in metabolic activities and mechanisms of tumor invasion. Understanding these functional differences in both scRNA-seq and bulk RNA-seq data enhances our insight into the mechanisms of OC progression.

Identification of hypermetabolic MPCs

To further investigate the specific functions of different clusters, we constructed metabolic profiles for MPCs (Fig. 3A). MPC5 exhibited the highest metabolic activity across

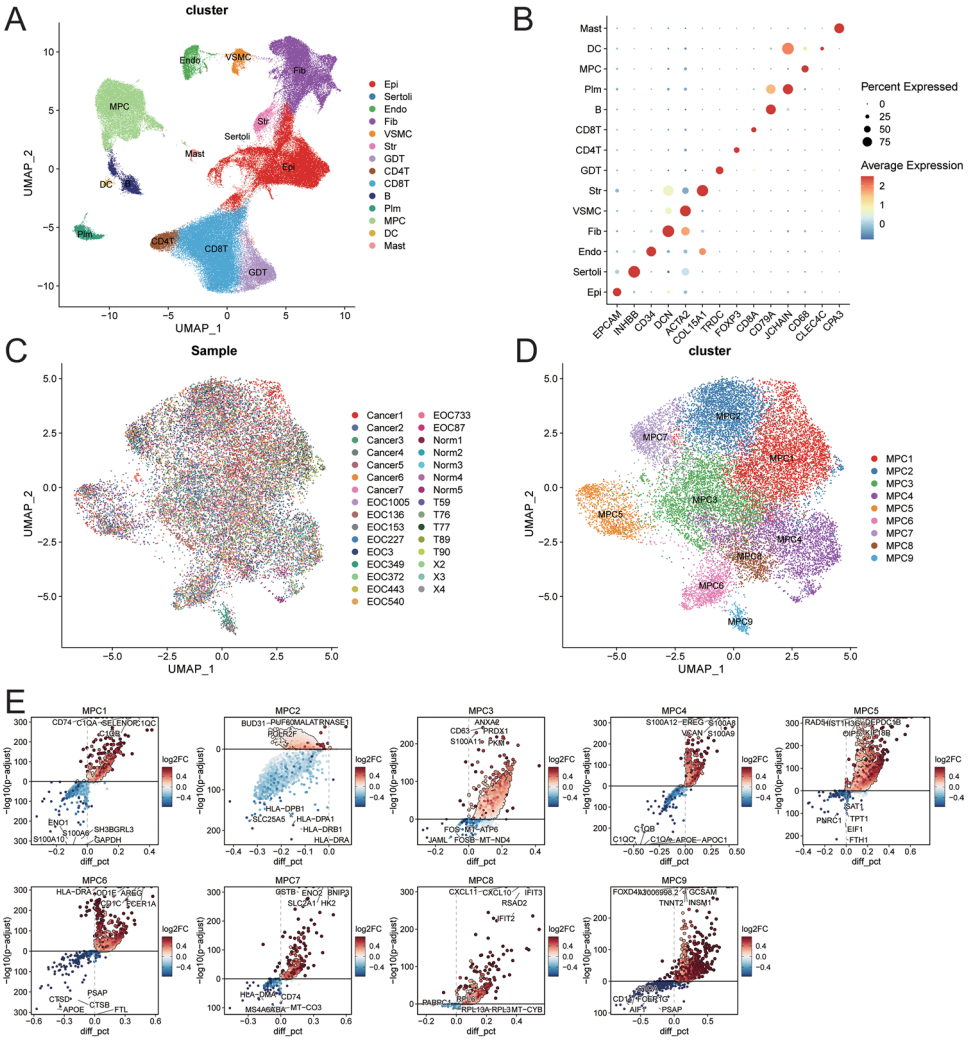

Fig. 1 Single-cell transcriptomic landscape of mononuclear phagocyte clusters in ovarian cancer. (**A**) UMAP dimensionality reduction visualization of 136,193 high-quality single cells from four integrated ovarian cancer datasets, colored by 14 distinct cell types identified through marker gene annotation. MPC: mononuclear phagocytes; DC: dendritic cells; CD8T: CD8 + T cells; CD4T: CD4 + T cells; GDT: gamma delta T cells; VSM: vascular smooth muscle cells; Str: stromal cells; Endo: endothelial cells; Fib: fibroblasts; Plm: plasma cells; Mast: mast cells; Sertoli: Sertoli cells. (**B**) Bubble plot showing the expression levels (color intensity) and percentage of expressing cells (bubble size) of canonical marker genes across the 14 identified cell clusters. (**C**) UMAP visualization of 19,544 mononuclear phagocyte cells after subclustering analysis, colored by sample origin, demonstrating the distribution of MPCs across datasets. (**D**) UMAP visualization of the 19,544 MPC cells, colored by 9 distinct MPC subclusters (MPC1-MPC9) identified at resolution 0.3. (**E**) Volcano plots displaying differentially expressed genes between selected MPC subclusters. Red dots indicate significantly upregulated genes (|avg_log2FC| > 0.5, FDR < 0.05); blue dots indicate significantly downregulated genes; and gray dots represent non-significant genes

all clusters, showing robust involvement in pathways such as the TCA cycle, fatty acid metabolism, and amino acid metabolism, followed by MPC7 and MPC3. Given the connection between energy metabolism and cell invasion in the TME, our focus was on the three hypermetabolic clusters: MPC3, MPC5, and MPC7. KEGG pathway analysis (Fig. 3B) indicated that these clusters were predominantly associated with hypoxia and glycogen metabolism-related signaling pathways, including the HIF-1, glucagon, and phosphatidylinositol signaling pathways. GSVA analysis of Hallmark gene sets further underscored the importance of these clusters in cellular metabolism (Fig. 3C). Reactome pathway analysis also highlighted that MPC3, MPC5, and MPC7 were the most enriched

Fig. 2 Functional characterization of different mononuclear phagocyte clusters. (**A**) Heatmap showing the expression levels of representative marker genes across the 9 MPC subclusters. Color intensity represents gene expression levels (red: high expression; blue: low expression). Clusters MPC1, MPC4, MPC6, MPC8, and MPC9 are predominantly enriched in immune response pathways, while MPC3, MPC5, and MPC7 are enriched in metabolic and proliferative pathways. (**B**) Word cloud plot visualizing the most significantly enriched biological processes in each MPC subcluster. Word size reflects the enrichment significance. (**C**) Word cloud plot displaying the top marker genes for each MPC subcluster. Word size corresponds to gene expression level or statistical significance

clusters (Fig. 3D). In summary, our results suggest that MPC3, MPC5, and MPC7 are highly metabolic macrophage clusters in OC, displaying metabolic reprogramming features that are associated with tumorigenesis and progression of OC.

Transcriptional regulation and developmental trajectory analysis of MPCs

Furthermore, transcription factors enriched in each subpopulation were identified based on their areas under the curve (AUC) scores (Fig. 4A). In MPC3, ZNF574, an oncogene in OC by regulating the AKT and AMPK pathways, was notably enriched, potentially serving as a prognostic marker and therapeutic target [28]. In MPC5, BRCA1, OVOL2, and CNOT3 were enriched. Numerous studies confirmed the association of BRCA1/2 mutations with OC [29]. In MPC7, ATF5, HSF4, and BARX1 were enriched. ATF5 dysfunction considerably enhanced OC cell apoptosis, making it a potential therapeutic target for epithelial OC [30]. In MPC9, CDX2, TBX21, and RELB were enriched. CDX2 potentially served as a prognostic biomarker for OC [31].

To better understand the changes in macrophages across disease stages, Slingshot was utilized to model the developmental trajectories of the 9 tumor cell clusters (Fig. 4B).

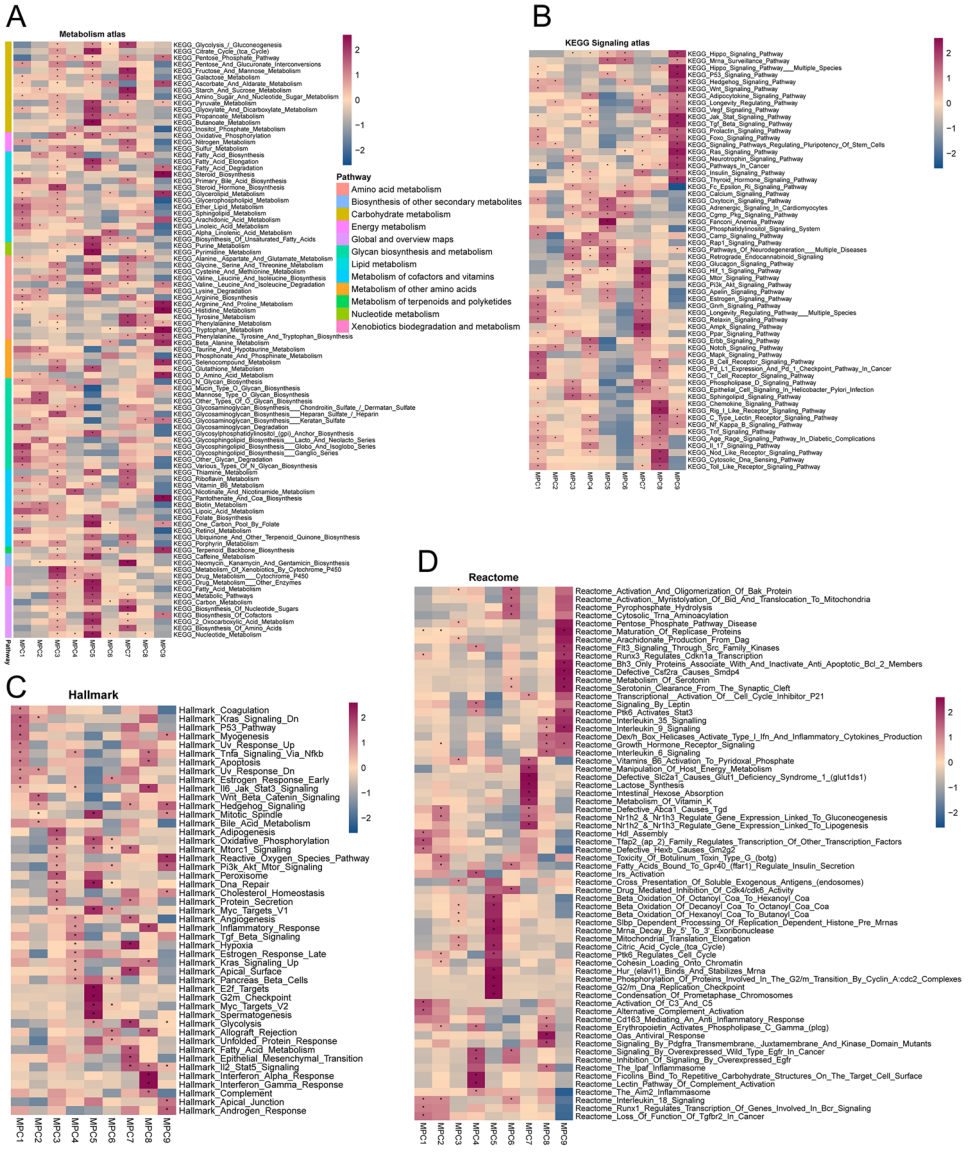

Fig. 3 Metabolic pathway enrichment analysis of mononuclear phagocyte clusters. (**A**) Heatmap of KEGG metabolic pathway enrichment scores across the 9 MPC subclusters. Color intensity represents the degree of pathway enrichment. MPC5 exhibits the highest metabolic activity and is strongly enriched in TCA cycle, fatty acid metabolism, and amino acid metabolism pathways, followed by MPC7 and MPC3. (**B**) Heatmap of KEGG signaling pathway enrichment scores across MPC subclusters. Hypermetabolic clusters (MPC3, MPC5, MPC7) are notably enriched in hypoxia-related pathways (HIF-1 signaling), glucagon signaling, and phosphatidylinositol signaling pathways. (**C**) Heatmap of Hallmark gene set enrichment scores across MPC subclusters, further confirming the elevated metabolic activity in MPC3, MPC5, and MPC7. **Asterisks indicate statistically significant enrichment (*$p < 0.05$; **$p < 0.01$; *$p < 0.001$). (**D**) Heatmap of Reactome pathway enrichment scores across MPC subclusters, highlighting the enrichment of metabolic reprogramming-related pathways in hypermetabolic clusters

Five differentiation states were represented by different colors. Combined with previous functional analyses, the results indicated that the initial monocyte-like cells predominantly differentiated into MPC3, MPC5, and MPC7 clusters along lineages 1, 2, and 3, exhibiting macrophage-like characteristics, while a smaller proportion differentiated into MPC6 and MPC9 along lineages 4 and 5, showing dendritic cell-like features (Fig. 4C). Collectively, high-energy metabolism is crucial in tumor invasion, and TAMs are important end-effector cells.

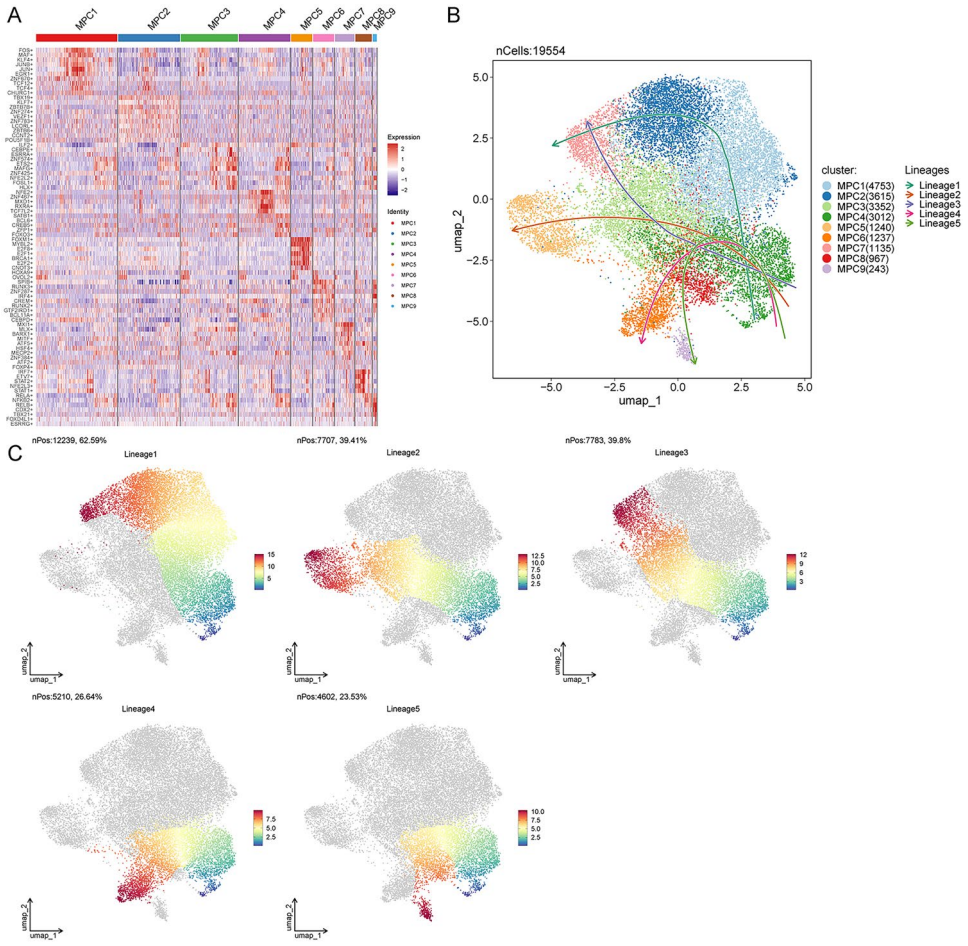

Fig. 4 Transcriptional regulation and developmental trajectory analysis of mononuclear phagocyte clusters. (**A**) Heatmap showing the relative activity scores of key transcription factors across the 9 MPC subclusters. Red indicates high transcriptional regulatory activity, while blue indicates low activity. Notable transcription factors enriched in hypermetabolic clusters include ZNF574 (MPC3), BRCA1 (MPC5), and ATF5 (MPC7). (**B**) Two-dimensional projection of the pseudotime developmental trajectories inferred by Slingshot analysis for the 9 MPC subclusters. Each point represents a single cell, colored by differentiation state along the inferred lineages. (**C**) Individual visualization of five distinct developmental lineages (Lineages 1–5) showing the differentiation paths from progenitor-like cells (MPC4, monocyte-like) toward terminal states, including macrophage-like clusters (MPC3, MPC5, MPC7) and dendritic cell-like clusters (MPC6, MPC9). Lineages are overlaid on the UMAP embedding from Fig. 4B

Cell-cell communication analysis

Cell-to-cell communication analysis was conducted across all cell clusters (Fig. 5A). MPC5, MPC7, and MPC9 clusters closely interacted with tumor epithelial cells. SPP1 and ALCAM pathways were notably increased in the tumor group (Fig. 5B). MPC5 and MPC7 showed significant communication in the tumor group compared to other clusters (Fig. 5C-D). Within MPC5 and MPC7 cells, SPP1 and FN1 pathways were notably enriched (Fig. 5E-F). In MPC5, the SPP1-CD44 interaction was significantly enhanced, which activated multiple ligand-receptor pairs, such as MIF-(CD74 + CXCR4) and FN1-CD44 (Fig. 5G-H). In MPC7, the SPP1-CD44 interaction was also greatly increased, along with the activation of additional ligand-receptor pairs such as MIF-(CD74 + CD44) and COL1A2-CD44 (Fig. 5I-J). Functional enrichment and scRNA-seq data revealed the involvement of SPP1 + TAMs in metastasis, angiogenesis, and cancer stem cell activation [32]. The SPP1 + TAM subpopulation was initially identified in colorectal

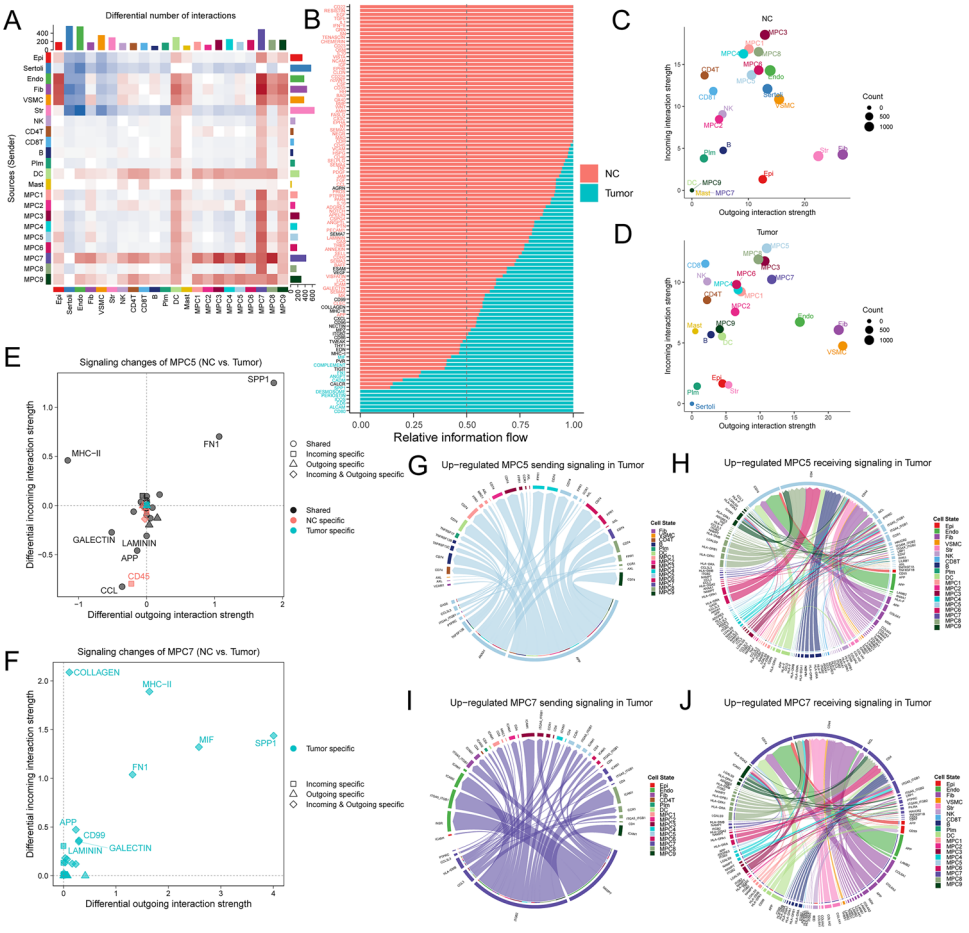

Fig. 5 Cell-cell communication networks between mononuclear phagocyte clusters and other cell types in thetumor microenvironment of ovarian cancer. (**A**) Heatmap showing the differential number of interactions between source cells (x-axis) and target cells (y-axis) across all identified cell types. Warmer colors indicate a higher number of predicted ligand-receptor interactions. (**B**) Relative information flow of signaling pathways differentially enriched between tumor and normal tissue conditions. Pathways with greater information flow in tumor samples are shown in red, while those enriched in normal samples are shown in blue. (**C**) Scatter plot comparing interaction strength between normal (NC) and tumor conditions for each MPC cluster. The x-axis represents outgoing interaction strength, while the y-axis represents outgoing interaction strength. Each circle represents an MPC cluster. (**D**) Scatter plot showing outgoing interaction strength for each MPC cluster. The x-axis represents outgoing interaction strength, while the y-axis represents differential outgoing interaction strength. (**E**-**F**) Circle plots depicting signaling pathway changes (shared, incoming-specific, outgoing-specific) between normal and tumor conditions for MPC5 (**E**) and MPC7 (**F**). Circle size reflects the number of signaling pathways. (**G**-**H**) Circle plots showing upregulated ligand-receptor pairs in MPC5 for sending (**G**) and receiving (**H**) signaling in the tumor microenvironment. The outer circle represents different cancer types or cell populations, and the inner connections represent ligand-receptor interactions. Line thickness and color intensity indicate the strength of communication probability (darker/thicker lines represent higher interaction strength). Different colors represent distinct cell states as indicated in the legend. (**I**-**J**) Circle plots showing upregulated ligand-receptor pairs in MPC7 for sending (**I**) and receiving (**J**) signaling in the tumor microenvironment. Key interactions include SPP1-CD44, MIF-(CD74 + CXCR4), and FN1-CD44. Color scheme and line thickness follow the same annotations as in (**G**-**H**)

cancer [33] and later in lung and breast cancers [34, 35]. A subpopulation of SPP1 + TAMs was also presented in squamous lung cancer. SPP1 + macrophages were considerably enhanced in the TME, which was associated with poor prognosis in patients with squamous lung cancer [32]. Overall, cell-to-cell communication patterns are markedly distinct among different MPCs in tumor tissue, and this heterogeneity may be related to OC progression.

Immune TME of hypermetabolic MPCs

The proportions of 14 single-cell compositions were calculated in 379 OC patients from the TCGA dataset using BayesPrism (Fig. 6A). Based on marker genes of different MPCs, samples were grouped to examine differences in immune cell infiltration. In MPC3, fibroblasts, CD4 T cells, and dendritic cells were greatly elevated in the high-expression group (Fig. 6B). In MPC5, dendritic cells were notably increased in the low-expression group (Fig. 6C). CD4 T cells were greatly elevated in the high-expression group. In MPC7, B cells were significantly higher in the low-expression group (Fig. 6D). MPC3 was positively correlated with fibroblasts, B cells, CD4 T cells, CD8 T cells, dendritic cells, and gamma delta T cells (Fig. 6E). MPC5 showed negative correlations with

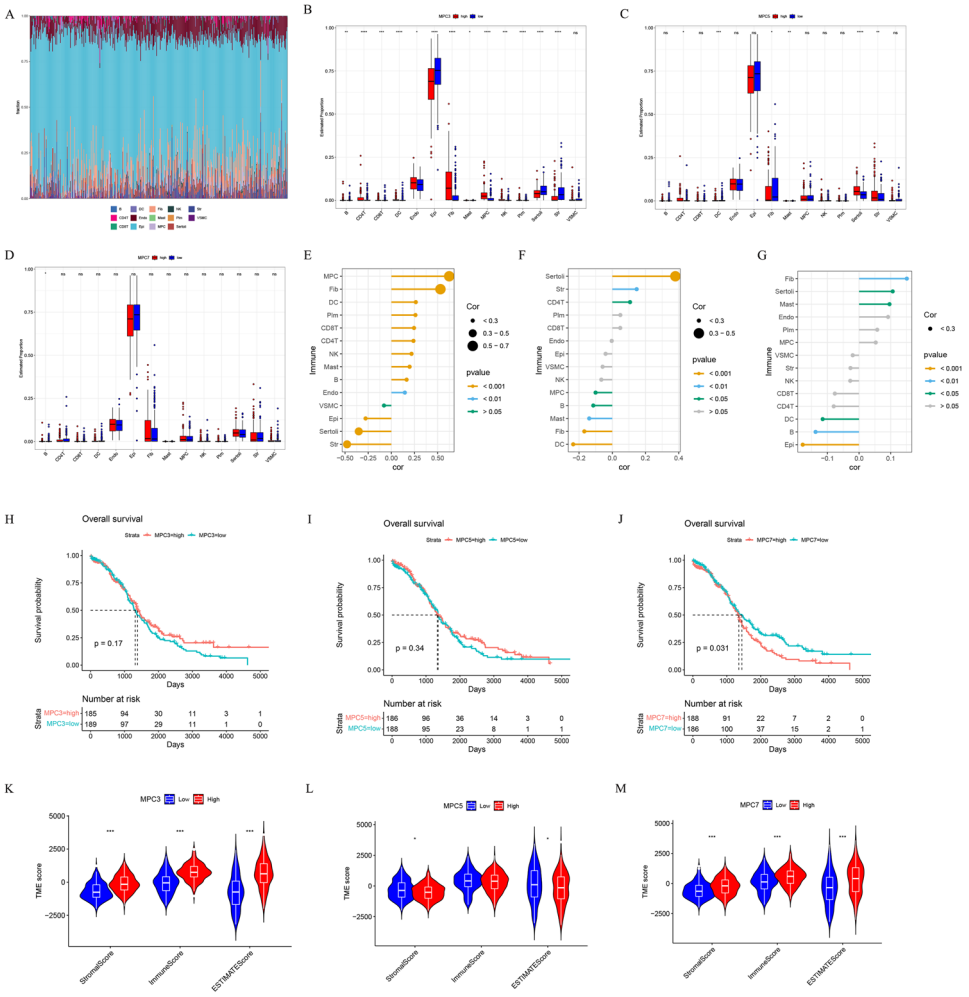

Fig. 6 Immune tumor microenvironment characterization of hypermetabolic mononuclear phagocyte clusters. (**A**) Stacked bar plot showing the inferred proportions of 14 immune and stromal cell types in 379 TCGA-OV patient samples using BayesPrism deconvolution, based on the single-cell reference from Fig. 1. (**B**-**D**) Boxplots comparing the abundance of immune cell types between high-expression and low-expression groups for MPC3 (**B**), MPC5 (**C**), and MPC7 (**D**). Significance levels: *$p < 0.05$; **$p < 0.01$; ***$p < 0.001$; ns: not significant. (**E**-**G**) Lollipop plots showing the correlation between MPC3 (**E**), MPC5 (**F**), and MPC7 (**G**) expression and the abundance of various immune cell types. The x-axis represents the correlation coefficient, and dot size reflects the absolute correlation strength. Dot color represents the p-value. (**H**-**J**) Kaplan–Meier survival curves comparing overall survival between high-expression and low-expression groups for MPC3 (**H**), MPC5 (**I**), and MPC7 (**J**) in the TCGA-OV cohort. The log-rank test p-value is shown for each comparison. (**K**-**M**) Boxplots comparing tumor purity, StromalScore, ImmuneScore, and ESTIMATEScore between high-expression and low-expression groups for MPC3 (**K**), MPC5 (**L**), and MPC7 (**M**). High-expression groups in all three clusters show higher tumor purity compared to low-expression groups

dendritic cells, fibroblasts, and mast cells (Fig. 6F). MPC7 was positively correlated with fibroblasts but negatively correlated with B cells and dendritic cells (Fig. 6G). Survival analysis indicated no significant differences in OS between the high- and low-expression groups in MPC3 and MPC5 (Fig. 6H-I), while the high-expression group in MPC7 had poorer OS (Fig. 6J). Furthermore, StromalScore, ImmuneScore, and ESTIMATEScore were calculated for MPC3, MPC5, and MPC7 using the Estimate tool. Results showed that the high-expression groups in these clusters had higher tumor purity than the low-expression groups (Fig. 6K-M).

MPC metabolism-related signature prognostic model

DEGs were identified from MPC3, MPC5, and MPC7 cells, and LASSO regression refined the list of candidate genes (Fig. 7A-B). Afterward, univariate Cox regression identified 10 genes significantly associated with prognosis (Fig. 7C), including CH25H, SLC7A11, RETN, NRGN, GPAT3, CCR7, TNS1, ISG20, UBD, and RAMP1. Based on these genes, risk score could be calculated: Risk score = 0.405*CH25H – 0.277*SLC7A11 + 0.509*RETN – 0.142*NRGN + 0.539*GPAT3–0.508*CCR7 + 0.211*TNS1–0.248*ISG20–0.184*UBD + 0.191*RAMP1. The ROC curve analysis demonstrated an AUC of 0.616 for 1-year OS and 0.714 for 3-year OS, indicating robust prediction performance (Fig. 7D). Kaplan-Meier survival curves revealed that the high-risk group had worse prognoses ($P < 0.0001$) (Fig. 7E). Additionally, statistically significant differences were found between the high- and low-risk groups as stratified by the risk score (Fig. 7F and G). Similarly, in the GSE26712 dataset, this risk score still distinguished prognosis, confirming its predictive validity across datasets. (Supplementary Fig. 4). In univariate Cox regression analysis, riskScore, Stage, and Age were all associated with patient prognosis ($P < 0.05$). However, in the multivariate Cox regression analysis, after adjusting for other variables, the significance of Stage diminished ($P > 0.05$) and no longer reached statistical significance. This suggests that Stage may be influenced by other factors, whereas the effects of riskScore ($P < 0.001$) and Age ($P < 0.001$) remained relatively stable (Fig. 7H and I).

Discussion

The characterized single-cell transcriptomic landscape of macrophage clusters in OC enhances our understanding of cellular heterogeneity and functional diversity of the TME. The scRNA-seq data were integrated from four independent datasets, and 17 MPCs critical in tumor progression and immune modulation [6] were identified, including 9 macrophage subtypes, highlighting the complex immune responses in OC [7]. Our analysis showed unique transcriptional signatures of MPCs, with MPC3, MPC5, and MPC7 demonstrating particularly high metabolic activity [36]. Consistently, previous studies have demonstrated the metabolic plasticity of macrophages within the TME [37]. Our study demonstrates metabolic reprogramming in MPCs at the single-cell level in OC, revealing notable alterations in key pathways such as the TCA cycle, fatty acid metabolism, and amino acid metabolism. These metabolic shifts facilitate tumor proliferation and resistance to platinum-based chemotherapeutic agents. Specifically, the MPC5 subset, exhibiting elevated fatty acid metabolism, may be implicated in chemoresistance. These insights underscore that targeting metabolic pathways may be a novel therapeutic option to improve outcomes in OC patients.

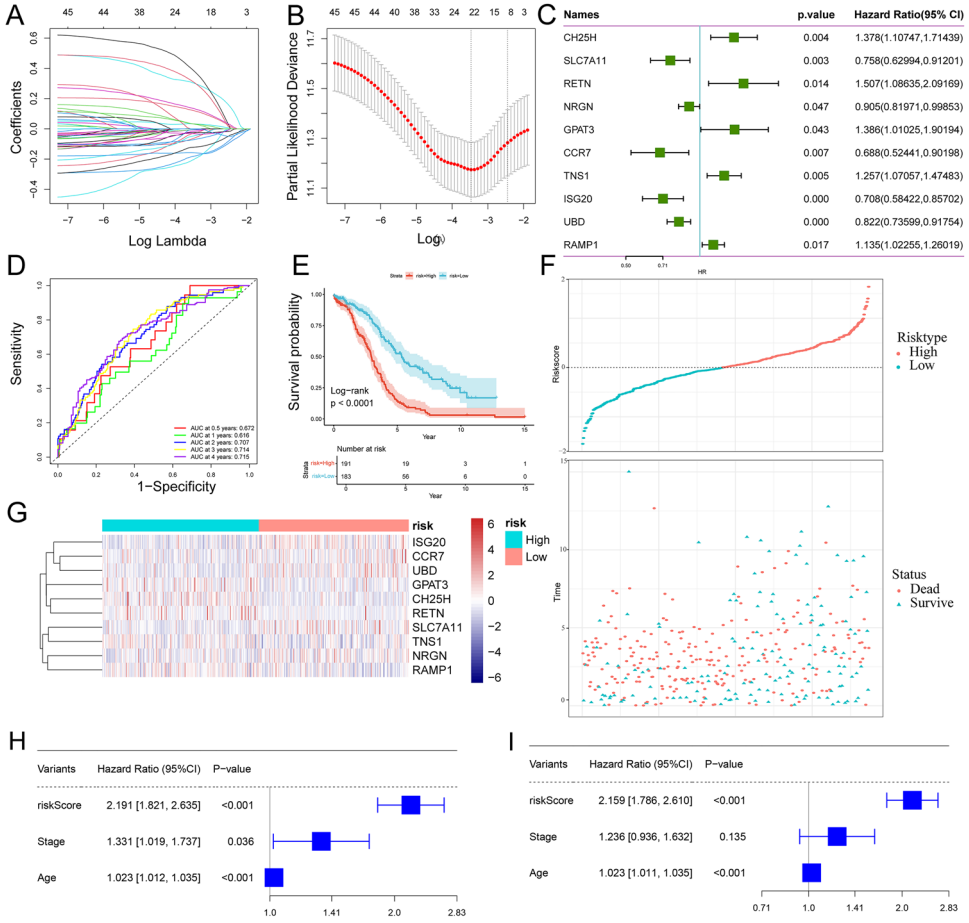

Fig. 7 Development and validation of an MPC metabolism-related prognostic risk model in ovarian cancer. (**A**) LASSO coefficient profiles of metabolism-related genes from MPC3, MPC5, and MPC7 across different log(λ) values. Each colored line represents the trajectory of an individual gene coefficient. (**B**) Partial likelihood deviance plot from LASSO Cox regression analysis for gene selection. The two vertical dashed lines indicate the optimal λ values: the left line corresponds to the λ value with minimum partial likelihood deviance (λ.min), and the right line corresponds to the λ value within one standard error of the minimum (λ.1se). The optimal log(λ) value (vertical dashed line) corresponding to the minimum partial likelihood deviance was used to select the most informative prognostic genes. (**C**) Forest plot showing the results of univariate Cox regression analysis for the 10 selected genes significantly associated with overall survival in the TCGA-OV cohort. Hazard ratios (HR) with 95% confidence intervals and p-values are displayed for each gene. (**D**) Time-dependent receiver operating characteristic (ROC) curves evaluating the predictive performance of the risk score for 0.5-, 1-, 2-, 3-, and 4-year overall survival. AUC values range from 0.5 to 1.0, with higher values indicating better predictive accuracy (AUC = 0.5 indicates random prediction, AUC = 1.0 indicates perfect prediction). (**E**) Kaplan–Meier survival curves comparing overall survival between high-risk and low-risk groups stratified by the median risk score in the TCGA-OV cohort. The log-rank test p-value indicates a significant survival difference between groups. (**F**) Risk factor plot showing the distribution of risk scores (top panel) for individual patients in the TCGA-OV cohort, ordered by increasing risk score. The dashed line indicates the median cut-off between high-risk and low-risk groups. (**G**) Heatmap showing the expression levels of the 10 model genes in high-risk and low-risk groups. Color scale represents relative gene expression (red: high expression; blue: low expression). (**H**) Forest plot from univariate Cox regression analysis evaluating the prognostic value of risk score, stage, and age. (**I**) Forest plot from multivariate Cox regression analysis adjusting for risk score, stage, and age. Risk score and age remained independent prognostic factors ($p < 0.001$), while no statistical significance for stage was found

Significant heterogeneity of macrophages was observed among MPCs in OC, with MPC3, MPC5, and MPC7 exhibiting distinct roles in metabolic reprogramming, cell proliferation, and tumor invasion [10]. Macrophages within the TME are not homogeneous but exhibit diverse phenotypes from pro-inflammatory to immunosuppressive types [38]. Macrophage heterogeneity is well-recognized as a key factor for tumor

growth, metastasis, and immune evasion [39]. Our study highlighted diverse functions of macrophage subtypes, shedding light on their distinct contributions to OC pathogenesis [40]. MPCs in OC exhibited significant heterogeneity across function, signaling, metabolism, interaction, and prognostic impact. MPC subgroups were involved in immune response, cell cycle regulation, and metabolic processes and differentially enriched in IL-17, HIF-1, and TNF pathways. MPC5 showed high activities in the TCA cycle and fatty acid metabolism, contributing to tumor growth and chemoresistance. MPCs interacted differently with tumor cells and immune cells, among which MPC5 and MPC7 were closely related to tumor invasion. Additionally, MPC7 was associated with worse OS. Targeting these specific subclusters may represent potential anti-tumor options.

GO, KEGG, and WikiPathway analyses uncovered that these MPCs were involved in distinct biological processes during tumor progression [41]. MPC1, MPC4, MPC6, MPC8, and MPC9 were primarily involved in immune responses, while MPC3, MPC5, and MPC7 were implicated in metabolic pathways [5]. Notably, MPC5 showed high enrichment in cell cycle and DNA replication pathways, suggesting its promoting role in tumor cell proliferation [42]. Similarly, an earlier study has demonstrated that TAMs support cancer cell proliferation by releasing cytokines and regulating the cell cycle [8].

MPC3, characterized by high metabolic activities, was enriched in the TNF and IL-17 pathways, suggesting its involvement in inflammatory responses and metabolic reprogramming [43]. Similarly, MPC7 exhibited strong associations with hypoxia and glycolysis-related signaling pathways, further emphasizing the role of metabolic reprogramming in driving tumor progression [44]. Research has confirmed the link between metabolic pathways and tumor invasion because cancer cells often experience metabolic shifts to support their rapid growth and evade immune surveillance [9].

Hypermetabolic clusters, particularly MPC3, MPC5, and MPC7, may be novel approaches for targeting the metabolic vulnerabilities of OC. The metabolic reprogramming observed in these clusters may result from the hypoxic TME, which drives the switch from oxidative phosphorylation to glycolysis [45]. This phenomenon, known as the Warburg effect, is well documented in cancer research as a hallmark of aggressive tumors [46].

The transcriptional regulation of MPCs provides valuable insights into key transcription factors that drive their differentiation and functional specialization. Our analysis identified key transcription factors, such as ZNF574 in MPC3, BRCA1 in MPC5, and ATF5 in MPC7, which are involved in OC progression [47]. For instance, BRCA1, a well-established tumor suppressor, is critical in DNA repair and cell cycle regulation, and its mutations are strongly linked to a high risk of OC [48]. The enrichment of BRCA1 in MPC5 suggests that this cluster may contribute to tumor progression through defects in DNA-repair pathways [12].

The analysis of developmental trajectories revealed that MPCs differentiated into distinct macrophage subtypes along multiple lineages [49]. MPC4, for example, differentiated into macrophage-like cells (MPC3, MPC5, and MPC7) and dendritic cell-like cells (MPC6 and MPC9) [50]. These findings suggest that macrophage plasticity within the TME may be a key driver of immune evasion and tumor progression [51]. Previous studies have highlighted that TAMs can transform into diverse phenotypes in response to TME signals, which further supports that macrophages can switch between pro-tumorigenic and anti-tumorigenic states under specific circumstances [52].

Cell-cell communication analysis using CellChat revealed intricate signaling networks between MPCs and tumor epithelial cells. MPC5, MPC7, and MPC9 tightly interacted with tumor epithelial cells, particularly through the SPP1 and ALCAM signaling pathways [53]. The increased communication in tumor cells underscores the importance of these pathways in facilitating tumor growth and metastasis [54]. Notably, the SPP1-CD44 interaction was significantly enriched in both MPC5 and MPC7, suggesting that these clusters may contribute to tumor cell invasion and immune suppression [55].

The ligand-receptor pairs MIF-(CD74 + CXCR4) and FN1-CD44 were activated, which highlighted the role of MPCs in suppressing the immune response and promoting tumor cell survival [56]. Consistently, previous evidence has confirmed that TAMs can promote tumor progression by secreting pro-tumorigenic cytokines and growth factors [57]. Targeting these cell-cell communication networks may be a promising strategy for disrupting the supportive role of macrophages in OC progression [58].

The correlations between MPCs and various immune cell types provide further insight into the complex interactions within the TME. For example, MPC3 was positively linked to fibroblasts, which are known to promote tumor progression by secreting pro-inflammatory cytokines [6]. In contrast, MPC5 exhibited a negative correlation with DC cells, which are typically associated with immune suppression [47].

The prognostic model based on DEGs in MPC3, MPC5, and MPC7 may advance personalized medicine in OC. The metabolic genes, such as CH25H, SLC7A11, and RETN, highlight the importance of metabolism in determining patient outcomes. The risk score derived from these genes could stratify patients into high- and low-risk groups, thus potentially guiding therapeutic decisions in clinical practice.

While our sc-RNA-seq analysis revealed the metabolic reprogramming characteristics of TAM clusters in OC and identified potential therapeutic targets and prognostic models, these findings still need to be substantiated through in vitro cell cultures, animal models, or clinical samples to ascertain their biological functions and therapeutic efficacy of prognostic genes. Moreover, the heterogeneity within our dataset may have affected the consistency and interpretability of the analytical results. Therefore, future studies with larger and more diverse patient cohorts are warranted to ensure broader clinical relevance and applicability of these findings. Additional experimental validation and datasets will enhance the assessment accuracy of the influence of metabolic reprogramming in OC progression and provide a more solid foundation for developing novel therapeutic strategies and prognostic tools.

Conclusion

Our study comprehensively analyzes the single-cell transcriptomic landscape of macrophage clusters in OC, revealing significant heterogeneity and diverse functions among MPCs. These hypermetabolic clusters, such as MPC3, MPC5, and MPC7, underscore the importance of metabolic reprogramming in driving tumor progression. Our findings highlight the critical role of cell-cell communication and immune modulation in shaping the TME, offering new ideas for the mechanisms of OC progression. The prognostic model based on MPC metabolism-related signatures represents a promising step toward personalized medicine in OC. Future investigations should further elucidate the molecular mechanisms of macrophage heterogeneity and explore novel therapeutic strategies targeting metabolic vulnerabilities in OC.

Supplementary Information

The online version contains supplementary material available at https://doi.org/10.1186/s13040-026-00542-4.

Supplementary Material 1: Supplementary Fig. 1. Quality control and batch effect correction of single-cell RNA sequencing data from ovarian cancer samples. (A) UMAP visualization of 136,193 single cells from four ovarian cancer datasets before batch effect correction, colored by cluster. (B) UMAP visualization of the same cells before batch effect correction, colored by original dataset origin (GSE154600, GSE158937, GSE184880, GSE165897). (C) UMAP visualization after batch effect correction using reciprocal principal component analysis, colored by cluster. (D) UMAP visualization after batch effect correction, colored by original dataset origin, demonstrating effective removal of batch effects

Supplementary Material 2: Supplementary Fig. 2. Optimization of clustering resolution for mononuclear phagocyte subpopulation identification. Line plot showing the trade-off between clustering resolution (0.25 to 1.20), the number of identified clusters (right y-axis), and the average silhouette score (left y-axis). The optimal resolution of 0.3 (red dashed line) was selected based on the balance between cluster separation (silhouette score) and granularity (cluster count), yielding 9 distinct MPC clusters

Supplementary Material 3: Supplementary Fig. 3. Gene regulatory networks and enriched biological processes in mononuclear phagocyte subpopulations. Supplementary Fig. 3 depicts the regulatory gene networks of nine mononuclear phagocyte clusters (MPCs) in ovarian cancer: (A) MPC1, (B) MPC2, (C) MPC3, (D) MPC4, (E) MPC5, (F) MPC6, (G) MPC7, (H) MPC8, and (I) MPC9. Nodes represent cluster-specific genes, and edges indicate functional associations. Gene Ontology Biological Process (GO BP) enrichment analysis highlights distinct functional programs across MPC subpopulations, including antigen processing and presentation and complement activation in MPC1–MPC2, monocyte-like immune features in MPC4, inflammatory and metabolically active tumor-associated macrophage characteristics in MPC3, highly proliferative and hypermetabolic programs in MPC5, hypoxia- and glycolysis-associated inflammatory signaling in MPC7, and dendritic cell–like immune regulatory functions in MPC6, MPC8, and MPC9, collectively revealing pronounced functional heterogeneity of MPCs within the microenvironment of ovarian cancer

Supplementary Material 4: Supplementary Fig. 4. Validation of the MPC metabolism-related prognostic risk model in the GSE26712 cohort. (A) Kaplan–Meier survival curves comparing overall survival between high-risk and low-risk groups stratified by the MPC metabolism-related risk score in the GSE26712 dataset ($n = 153$). The log-rank test p-value indicates a significant survival difference between groups. (B) Time-dependent receiver operating characteristic (ROC) curves evaluating the predictive performance of the risk score for 1-, 2-, 3-, 4-, and 5-year overall survival. AUC values range from 0.5 to 1.0, with higher values indicating better predictive accuracy (AUC = 0.5 indicates random prediction, AUC = 1.0 indicates perfect prediction). (C) Risk factor plot showing the distribution of risk scores (top), survival status (middle), and expression heatmap of the 10 model genes (bottom) for individual patients in the GSE26712 cohort. Patients are ordered by increasing risk score. The vertical dashed line indicates the median cut-off between high-risk and low-risk groups

Acknowledgements
Not applicable.

Author contributions
Lin Qi: Conceptualization, Methodology, Investigation, Writing - Original Draft, Funding acquisition; Li Li: Investigation, Formal analysis, Data Curation, Writing - Original Draft; Yinuo Liu: Methodology, Validation, Resources Formal analysis; Wenshu Li: Software, Formal analysis, Visualization; Yaru Ma: Writing - Review & Editing, Supervision, Project administration, Data Curation; Manyin Zhao: Conceptualization, Supervision, Project administration, Funding acquisition, Writing - Review & Editing.

Funding
This work was supported by the Youth Fund of Yantai Yuhuangding Hospital (QN202404 for Lin Qi).

Data availability
The datasets supporting this study are publicly available in the GitHub repository (Release v1.0.0; https://github.com/shenshou70/code-OC/releases/tag/v1.0.0), including MPC.qs, list_human.qs, and RNA.rar. All analysis code is available in the main branch of the same repository (https://github.com/shenshou70/code-OC). Raw data were obtained from the GEO database (GSE154600, GSE158937, GSE184880, GSE165897, and GSE26712) and TCGA.

Declarations

Ethics approval and consent to participate
Not applicable.

Consent for publication
Not applicable.

Competing interests
The authors declare no competing interests.

Received: 9 May 2025 / Accepted: 14 March 2026
Published online: 03 April 2026

References

1. Surveillance HS, Research ACS, Atlanta G, Surveillance HS, Research ACS. Atlanta, Georgia., Surveillance, Health Services Research ACS, Atlanta, Georgia.: Cancer statistics, 2020. Cancer J Clin. 2020;70(1):7–30.
2. Webb PM, Jordan SJ. Epidemiology of epithelial ovarian cancer. Best Pract Res Clin Obstet Gynecol. 2016;41:3–14.
3. A TL, Britton T, E DC, D MK, Goli S, D RC, M GM, Ahmedin J, L SR Ovarian cancer statistics, 2018. CA Cancer J Clin. 2018;68(4):284–296.
4. Ruffell B, Coussens LM. Macrophages and Therapeutic Resistance in Cancer. Cancer Cell. 2015;27(4):462–72.
5. Qian B-Z, Pollard JW. Macrophage Diversity Enhances Tumor Progression and Metastasis. Cell. 2010;141(1):39–51.
6. Alberto M, K BS, Rosaria GM, Antonio S, Massimo L. Macrophage plasticity and polarization in tissue repair and remodelling. J Pathol. 2013;229(2):176–85.
7. K BS, Alberto M. Macrophage plasticity and interaction with lymphocyte subsets: cancer as a paradigm. Nat Immunol. 2010;11(10):889–96.
8. Patel AP, Tirosh I, Trombetta JJ, Shalek AK, Gillespie SM, Wakimoto H, Cahill DP, Nahed BV, Curry WT, Martuza RL, et al. Single-cell RNA-seq highlights intratumoral heterogeneity in primary glioblastoma. Science. 2014;344(6190):1396–401.
9. Lavin Y, Kobayashi S, Leader A, Amir E-aD, Elefant N, Bigenwald C, Remark R, Sweeney R, Becker CD, Levine JH, et al. Innate Immune Landscape in Early Lung Adenocarcinoma by Paired Single-Cell Analyses. Cell. 2017;169(4):750–e765717.
10. Franklin RA, Liao W, Sarkar A, Kim MV, Bivona MR, Liu K, Pamer EG, Li MO. The cellular and molecular origin of tumor-associated macrophages. Science. 2014;344(6186):921–5.
11. Ostuni RKF, Murray PJ, Natoli G. Macrophages and cancer: from mechanisms to therapeutic implications. Trends Immunol. 2015;36(4):229–39.
12. G DD, Brian R. Macrophages as regulators of tumour immunity and immunotherapy. Nat Rev Immunol. 2019;19(6):369–82.
13. Condeelis J, Pollard JW. Macrophages: Obligate Partners for Tumor Cell Migration, Invasion, and Metastasis. Cell. 2006;124(2):263–6.
14. Lijuan S, Tim K, Santos AA, Bodu L, XueYan H, David N, Xiao H, L SD, Phyllis AMI. Activating a collaborative innate-adaptive immune response to control metastasis. Cancer Cell. 2021;39(10):1361–e13741369.
15. Luo Y, Xia Y, Liu D, Li X, Li H, Liu J, Zhou D, Dong Y, Li X, Qian Y, et al. Neoadjuvant PARPi or chemotherapy in ovarian cancer informs targeting effector Treg cells for homologous-recombination-deficient tumors. Cell. 2024;187(18):4905–e49254924.
16. Brian JGM, Mim C, Kristupas H, Fran R, Akhil M, Ayan K, Yunhai B, Dave L, N BA. Visualizing and interpreting cancer genomics data via the Xena platform. Nat Biotechnol. 2020;38(6):675–8.
17. Raphael P, Zhuliu L, Rui K. Machine learning and statistical methods for clustering single-cell RNA-sequencing data. Brief Bioinform. 2020;21(4):1209–23.
18. Andrew B, Paul H, Peter S, Efthymia P, Rahul S. Integrating single-cell transcriptomic data across different conditions, technologies, and species. Nat Biotechnol. 2018;36(5):411–20.
19. Congxue H, Tengyue L, Yingqi X, Xinxin Z, Feng L, Jing B, Jing C, Wenqi J, Kaiyue Y, Qi O, et al. CellMarker 2.0: an updated database of manually curated cell markers in human/mouse and web tools based on scRNA-seq data. Nucleic Acids Res 2022;51(D1).
20. Franzén OGL, Björkegren JLM. PanglaoDB: a web server for exploration of mouse and human single-cell RNA sequencing data. Database: The Journal of Biological Databases and Curation 2019;2019:baz046.
21. Guangchuang Y, Li-Gen W, Yanyan H, Qing-Yu H. clusterProfiler: an R package for comparing biological themes among gene clusters. OMICS. 2012;16(5):284–7.
22. K M, G S. KEGG: kyoto encyclopedia of genes and genomes. Nucleic Acids Res. 2000;28(1):27–30.
23. Street K, Risso D, Fletcher RB, Das D, Ngai J, Yosef N, Purdom E, Dudoit S. Slingshot: cell lineage and pseudotime inference for single-cell transcriptomics. BMC Genomics. 2018;19(1):477.
24. Jin S, Guerrero-Juarez CF, Zhang L, Chang I, Ramos R, Kuan CH, Myung P, Plikus MV, Nie Q. Inference and analysis of cell-cell communication using CellChat. Nat Commun. 2021;12(1):1088.
25. Long MNABSC, Florian LCJGAACA, David SSKMSEMALB. Determining cell type abundance and expression from bulk tissues with digital cytometry. Nat Biotechnol. 2019;37(7):773–82.
26. Kosuke Y, Maria S, Emmanuel M, Rahulsimham V, Hoon K, Wandaliz T-G, Victor T, Hui S, A LD. Inferring tumour purity and stromal and immune cell admixture from expression data. Nat Commun. 2013;4(1):2612.
27. Puisieux A, Pommier RM, Morel A-P, Lavial F. Cellular Pliancy and the Multistep Process of Tumorigenesis. Cancer Cell. 2018;33(2):164–72.
28. Jingjing Z, Xiaoli W, Li H. ZNF574 Promotes Ovarian Cancer Cell Proliferation and Migration through Regulating AKT and AMPK Signaling Pathways. Ann Clin Lab Sci. 2022;52(4):611–20.
29. B P: BRCA1- and BRCA2-related mutations: therapeutic implications in ovarian cancer. Annals oncology: official J Eur Soc Med Oncol. 2013;24 Suppl 8(suppl_8):viii22–7.
30. Aiping C, Dongmeng Q, Bin W, Ming H, Jinrong L, Yani Q, X LD. ATF5 is overexpressed in epithelial ovarian carcinomas and interference with its function increases apoptosis through the downregulation of Bcl-2 in SKOV-3 cells. Int J Gynecol pathology: official J Int Soc Gynecol Pathologists. 2012;31(6):532–7.
31. Wang L, Rambau PF, Kelemen LE, Anglesio MS, Leung S, Talhouk A, Köbel M. Nuclear β-catenin and CDX2 expression in ovarian endometrioid carcinoma identify patients with favourable outcome. Histopathology. 2019;74(3):452–62.
32. Wang J, Zhu N, Su X, Gao Y, Yang R. Novel tumor-associated macrophage populations and subpopulations by single cell RNA sequencing. Front Immunol. 2023;14:1264774–1264774.
33. Zhang L, Li Z, Skrzypczynska KM, Fang Q, Zhang W, O'Brien SA, He Y, Wang L, Zhang Q, Kim A, et al. Single-Cell Analyses Inform Mechanisms of Myeloid-Targeted Therapies in Colon Cancer. Cell. 2020;181(2):442–e459429.
34. Azizi E, Carr AJ, Plitas G, Cornish AE, Konopacki C, Prabhakaran S, Nainys J, Wu K, Kiseliovas V, Setty M, et al. Single-Cell Map of Diverse Immune Phenotypes in the Breast Tumor Microenvironment. Cell. 2018;174(5):1293–e13081236.
35. Kim NKH, Lee K, Hong Y, Cho JH, Choi JW, Lee JI, Suh YL, Ku BM, Eum HH, Choi S, Choi YL, Joung JG, Park WY, Jung HA, Sun JM, Lee SH, Ahn JS, Park K, Ahn MJ, Lee HO. Single-cell RNA sequencing demonstrates the molecular and cellular reprogramming of metastatic lung adenocarcinoma. Nat Commun. 2020;11(1):2285.
36. Noy R, Pollard JW. Tumor-Associated Macrophages: From Mechanisms to Therapy. Immunity. 2014;41(1):49–61.
37. Suzanne O-R, Pratima S. Myeloid-derived suppressor cells: linking inflammation and cancer. J Immunol (Baltimore Md: 1950). 2009;182(8):4499–506.

38. Lorenzo G, Aitziber B, Oliver K, Laurence Z, Guido K. Immunogenic cell death in cancer and infectious disease. Nat Rev Immunol. 2017;17(2):97–111.
39. Ginhoux F, Guilliams M. Tissue-Resident Macrophage Ontogeny and Homeostasis. Immunity. 2016;44(3):439–49.
40. Wynn TACA, Pollard JW. Macrophage biology in development, homeostasis and disease. Nature. 2013;496(7446):445–55.
41. Ruslan M. Origin and physiological roles of inflammation. Nature. 2008;454(7203):428–35.
42. Lichun M, Sophia H, Limin W, KF L, Subreen K, Marshonna F, Michael K, Areeba MHS. Multiregional single-cell dissection of tumor and immune cells reveals stable lock-and-key features in liver cancer. Nat Commun. 2022;13(1):7533–7533.
43. Aras SZM. TAMeless traitors: macrophages in cancer progression and metastasis. Br J Cancer. 2017;117(11):1583–91.
44. Siamon G, Annette P. Tissue macrophages: heterogeneity and functions. BMC Biol. 2017;15(1):53.
45. Gubin MM, Esaulova E, Ward JP, Malkova ON, Runci D, Wong P, Noguchi T, Arthur CD, Meng W, Alspach E, et al. High-Dimensional Analysis Delineates Myeloid and Lymphoid Compartment Remodeling during Successful Immune-Checkpoint Cancer Therapy. Cell. 2018;175(5):1443–1443.
46. Mikhail B, W RE, Kelly K, Vincent C, F FD, Miriam M, Suzanne MCLIGD, C O-R. Understanding the tumor immune microenvironment (TIME) for effective therapy. Nat Med. 2018;24(5):541–50.
47. Julie P, Mary R-H, Carrie E, Jacqueline K, Suryaprakash S. Innate immunity in aging: impact on macrophage function. Aging Cell. 2004;3(4):161–7.
48. Ilaria M, Luigi D, Paolo S, Paola Z, Vincenzo B. Tumor-induced tolerance and immune suppression by myeloid derived suppressor cells. Immunol Rev. 2008;222(1):162–79.
49. Paola A, Antonio S, Graziella S, Chiara P, Alberto M. The inflammatory micro-environment in tumor progression: the role of tumor-associated macrophages. Critical Reviews in Oncology/Hematology. 2008;66(1):1–9.
50. Papatriantafyllou M. STATs control subset-specific enhancer activation. Nat Rev Immunol. 2013;13(1):7–7.
51. Balkwill F, Mantovani A. Inflammation and cancer: back to Virchow? Lancet. 2001;357(9255):539–45.
52. E LC W. Distinct role of macrophages in different tumor microenvironments. Cancer Res. 2006;66(2):605–12.
53. Martha L-Y, Luca C, W PJ. Macrophage targeting in cancer. Ann N Y Acad Sci. 2020;1499(1):18–41.
54. Yuanyuan A, Qing Y. Tumor-associated macrophage targeted therapeutics in ovarian cancer. Int J Cancer. 2020;149(1):21–30.
55. Tan TZHV, Ye J, Lim D, Low J, Choolani M, Scott C, Tan DSP, Huang RY. Decoding transcriptomic intra-tumour heterogeneity to guide personalised medicine in ovarian cancer. J Pathol. 2019;247(3):305–19.
56. Katsutoshi O, Michihiro T, Kenbun S, Mayuyo M-U, Yutaka O, Tomoyuki F. Recent advances in targeting DNA repair pathways for the treatment of ovarian cancer and their clinical relevance. Int J Clin Oncol. 2017;22(4):611–8.
57. Nowak MKM. The Role of Tumor-Associated Macrophages in the Progression and Chemoresistance of Ovarian Cancer. Cells. 2020;9(5):1299–1299.
58. Yousefzadeh Y, Hallaj S, Moornani MB, Asghary A, Azizi G, Hojjat-Farsangi M, Ghalamfarsa G, Jadidi-Niaragh F. Tumor associated macrophages in the molecular pathogenesis of ovarian cancer. Int Immunopharmacol. 2020;84:106471.

Publisher's note